The von Hippel–Lindau Chuvash mutation promotes pulmonary hypertension and fibrosis in mice

Michele M. Hickey,[1,2,3] Theresa Richardson,[1,3] Tao Wang,[4,5] Matias Mosqueira,[6] Evguenia Arguiri,[5] Hongwei Yu,[1] Qian-Chun Yu,[1] Charalambos C. Solomides,[7] Edward E. Morrisey,[2,4,5] Tejvir S. Khurana,[2,6] Melpo Christofidou-Solomidou,[5] and M. Celeste Simon[1,2,3]

[1]Abramson Family Cancer Research Institute, [2]Cell and Molecular Biology Graduate Group, [3]Howard Hughes Medical Institute, [4]Cardiovascular Institute, [5]Department of Medicine, and [6]Department of Physiology and Pennsylvania Muscle Institute, University of Pennsylvania School of Medicine, Philadelphia. [7]Department of Pathology, Anatomy, and Cell Biology, Thomas Jefferson Medical College, Philadelphia.

Mutation of the von Hippel–Lindau (VHL) tumor suppressor protein at codon 200 (R200W) is associated with a disease known as Chuvash polycythemia. In addition to polycythemia, Chuvash patients have pulmonary hypertension and increased respiratory rates, although the pathophysiological basis of these symptoms is unclear. Here we sought to address this issue by studying mice homozygous for the R200W *Vhl* mutation (*Vhl*$^{R/R}$ mice) as a model for Chuvash disease. These mice developed pulmonary hypertension independently of polycythemia and enhanced normoxic respiration similar to Chuvash patients, further validating *Vhl*$^{R/R}$ mice as a model for Chuvash disease. Lungs from *Vhl*$^{R/R}$ mice exhibited pulmonary vascular remodeling, hemorrhage, edema, and macrophage infiltration, and lungs from older mice also exhibited fibrosis. HIF-2α activity was increased in lungs from *Vhl*$^{R/R}$ mice, and heterozygosity for *Hif2a*, but not *Hif1a*, genetically suppressed both the polycythemia and pulmonary hypertension in the *Vhl*$^{R/R}$ mice. Furthermore, *Hif2a* heterozygosity resulted in partial protection against vascular remodeling, hemorrhage, and edema, but not inflammation, in *Vhl*$^{R/R}$ lungs, suggesting a selective role for HIF-2α in the pulmonary pathology and thereby providing insight into the mechanisms underlying pulmonary hypertension. These findings strongly support a dependency of the Chuvash phenotype on HIF-2α and suggest potential treatments for Chuvash patients.

Introduction

Cellular adaptation to low oxygen, or hypoxia, is primarily mediated by the hypoxia-inducible factor (HIF) family of transcription factors. HIFs are heterodimers of an α and a β subunit that activate the expression of a broad range of targets involved in processes such as glycolysis, angiogenesis, and erythropoiesis (1). There are 2 primary HIF-α isoforms, HIF-1α and HIF-2α; HIF-1α regulates the expression of glycolytic enzyme genes including phosphoglycerate kinase (*PGK1*), whereas HIF-2α activates the expression of erythropoietin (*EPO*) (2–4). In addition, a number of other targets are preferentially induced by HIF-2α in many cell types, such as vascular endothelial growth factor (*VEGFA*) and plasminogen activator inhibitor–1 (*SERPINE1*, also known as *PAI-1*) (2, 5, 6).

HIF activity is controlled through the regulation of α subunit protein stability by the von Hippel–Lindau (VHL) tumor suppressor protein (pVHL). pVHL functions as the substrate recognition component of an E3 ubiquitin ligase complex that targets HIF-α proteins for oxygen-dependent degradation (7–11). *VHL* mutations are typically associated with a hereditary cancer syndrome known as VHL disease, which is characterized by predisposition to the formation of highly vascular tumors within specific tissues (12). Loss of pVHL impairs HIF regulation, resulting in constitutive and inappropriate stimulation of HIF target genes (10). In addition, although most *VHL* mutations disrupt the HIF pathway, HIF-independent functions of pVHL are also important for tumor suppression, particularly the regulation of ECM assembly and control of apoptosis via suppression of JunB (13–16).

Unlike most *VHL* mutations, germline homozygosity for the 598C>T mutation in exon 3 does not result in tumor formation but rather is associated with development of Chuvash polycythemia. This autosomal recessive disease is endemic to the Chuvash region of Russia and the Italian island of Ischia but has also been found among patients of diverse ethnicities (17–24). Chuvash polycythemia is defined by increased hemoglobin and hematocrit, elevated serum levels of EPO, VEGF, and PAI-1, and hypersensitivity of erythroid progenitors to EPO (18, 19, 21, 22, 24). Furthermore, this form of polycythemia is associated with an enhanced risk of both hemorrhage and thrombosis, leading to premature mortality (19, 21, 25). The 598C>T transition results in substitution of tryptophan for arginine at codon 200 (R200W in humans) at the C terminus of pVHL; this residue is located in a region shown to stabilize the pVHL–HIF-α interaction and to promote complete HIF-α ubiquitination, suggesting that dysregulated HIF activity may play a role in this disease (17, 18, 26).

In addition to polycythemia, Chuvash patients are also susceptible to developing pulmonary hypertension (27, 28), which can be induced by hypoxia and is defined as an increase in resistance to blood flow due to vascular remodeling in the lung (29). It is often accompanied by the accumulation of ECM proteins and infiltration of immune cells and can eventually lead to compensatory hypertrophy of the RV wall of the heart (29–31). Dysregulated expression of many HIF targets, including endothelin-1 (*EDN1*, also known as *ET-1*), *SERPINE1*, and platelet-derived growth factor–β (*PDGFB*), promotes pulmonary hypertension, inflammation,

Conflict of interest: The authors have declared that no conflict of interest exists.
Citation for this article: *J Clin Invest.* 2010;120(3):827–839. doi:10.1172/JCI36362.

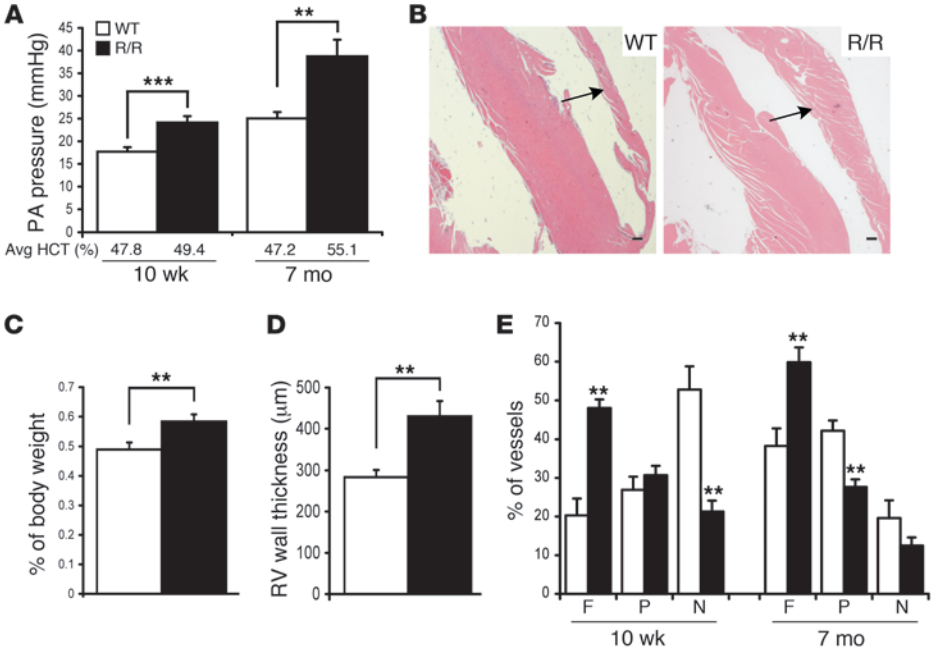

Figure 1

Vhl$^{R/R}$ (R/R) mice develop pulmonary hypertension. (**A**) Systolic PA pressure was increased 1.5-fold in older, polycythemic *Vhl*$^{R/R}$ mice (7 months of age) compared with WT controls (n = 12–13 per genotype). Elevated PA pressure was already present in 10-week-old *Vhl*$^{R/R}$ mice (1.4-fold greater, n = 20–25), prior to any significant increase in hematocrit (HCT) levels and the onset of polycythemia (**P < 0.001, ***P < 0.0004). (**B**) *Vhl*$^{R/R}$ hearts displayed RV hypertrophy (arrows) by 7 months of age. (**C** and **D**) Heart/body weight ratios (**C**, n = 18–21) and RV wall thickness (**D**, n = 11–17) were both significantly increased in older *Vhl*$^{R/R}$ mice (1.2-fold and 1.5-fold greater, respectively, **P < 0.009). (**E**) The distribution of fully muscularized (F), partially muscularized (P), and nonmuscularized (N) vessels was shifted in *Vhl*$^{R/R}$ lungs at both ages, with an increased proportion of fully muscularized vessels and a decrease in nonmuscularized vessels compared with WT animals (n = 4–5 per genotype at each age, **P < 0.006). Scale bars: 300 μm.

and fibrosis in animal models and in human patients (32–37). Importantly, HIF activation has been shown to contribute to the pathogenesis of pulmonary hypertension in vivo, as heterozygosity for either *Hif1a* (38) or *Hif2a* (*Epas1*, referred to as *Hif2a* hereafter) (39) delays the development of this phenotype in mice exposed to chronic hypoxia. In particular, decreased HIF-2α levels result in lower pulmonary pressure, the absence of RV hypertrophy, and reduced expression of ET-1 (39). Furthermore, HIF-1α regulates pulmonary artery myocyte electrophysiology (40–42) and promotes the proliferation of vascular smooth muscle cells (43), whereas HIF-2α enhances the proliferation and migration of pulmonary artery fibroblasts (44).

In Chuvash patients, pulmonary arterial (PA) pressure is elevated nearly 2-fold at baseline, with average values of approximately 30–35 mmHg (27, 28). Exposure to hypoxia provokes a greater increase in PA pressure in these patients (5- to 10-fold over that of controls to values approaching 60 mmHg), as well as increased respiratory rates (approximately 2-fold greater) (27). Plasma ET-1 levels are also increased compared with those in controls, suggesting a role for HIF in this phenotype (28). However, the exact mechanisms underlying this disease are not well understood, and the contribution of HIF activity and relationship to polycythemia remain unknown. In addition, it is not known whether the hypertension in these patients is accompanied by other pulmonary pathologies.

We previously generated mice expressing the R200W point mutation from the endogenous *Vhl* locus (*Vhl*$^{R/R}$); these mice develop polycythemia highly similar to the human disease (45). Here we show that *Vhl*$^{R/R}$ mice also faithfully recapitulated the pulmonary hypertension and enhanced normoxic respiration observed in patients. Moreover, the R200W substitution resulted in additional pulmonary pathologies, including vascular remodeling, fibrosis, hemorrhage, edema, and macrophage recruitment. HIF-2α activity was upregulated in *Vhl*$^{R/R}$ lungs, and heterozygous expression of *Hif2a*, but not *Hif1a*, partially rescued most of these pulmonary phenotypes, as well as the polycythemia, in *Vhl*$^{R/R}$ mice. These results provide strong genetic evidence of the dependency of Chuvash disease on the HIF-2α isoform and suggest potential therapeutic strategies for treating patients.

Results

Vhl$^{R/R}$ *mice develop PA hypertension*. In order to quantitatively determine whether *Vhl*$^{R/R}$ mice developed pulmonary hypertension similar to Chuvash patients, we directly measured systolic PA pressure. As shown in Figure 1A, PA pressure was increased in older *Vhl*$^{R/R}$ mice (approximately 7 months old) compared with age-matched WT controls (38.7 ± 3.7 mmHg versus 25.0 ± 1.4 mmHg in WT mice, n = 12–13 measurements for each genotype, P < 0.001). *Vhl*$^{R/R}$ mice at this age are polycythemic (45), as evidenced by elevated hematocrit levels (Figure 1A, right, 55.1% versus 47.2% in WT mice, P < 0.0001). To investigate the relationship between the pulmonary hypertension and polycythemic phenotypes, we also determined PA pressure at 10 weeks of age, before there were significant changes in *Vhl*$^{R/R}$ hematocrit values (Figure 1A, 49.4% versus 47.8% in WT mice, NS: P < 0.2) (45). Pulmonary hypertension was also present in these younger animals (Figure 1A, 24.1 ± 1.4 mmHg versus 17.7 ± 1.0 mmHg in WT mice, n = 20–25 measurements, P < 0.0004), suggesting that the pulmonary phenotype develops prior to the onset and independently of polycythemia in *Vhl*$^{R/R}$ mice. Importantly, the magnitude of the increase in *Vhl*$^{R/R}$ PA pressure (approximately 1.5-fold) was similar to that observed in Chuvash patients (approximately 2-fold) (27, 28). These results demonstrate that, in addition to the polycythemic phenotype, *Vhl*$^{R/R}$ mice also recapitulate this pulmonary aspect of Chuvash disease.

RV hypertrophy frequently occurs as a compensatory mechanism in response to pulmonary hypertension in humans to maintain efficient blood flow to the lungs in the face of increased vascular resistance (31). Histologic analysis of *Vhl*$^{R/R}$ hearts revealed thickening of the RV wall in older mutant mice (7–8 months of age) compared with age-matched WT hearts (Figure 1B, arrows).

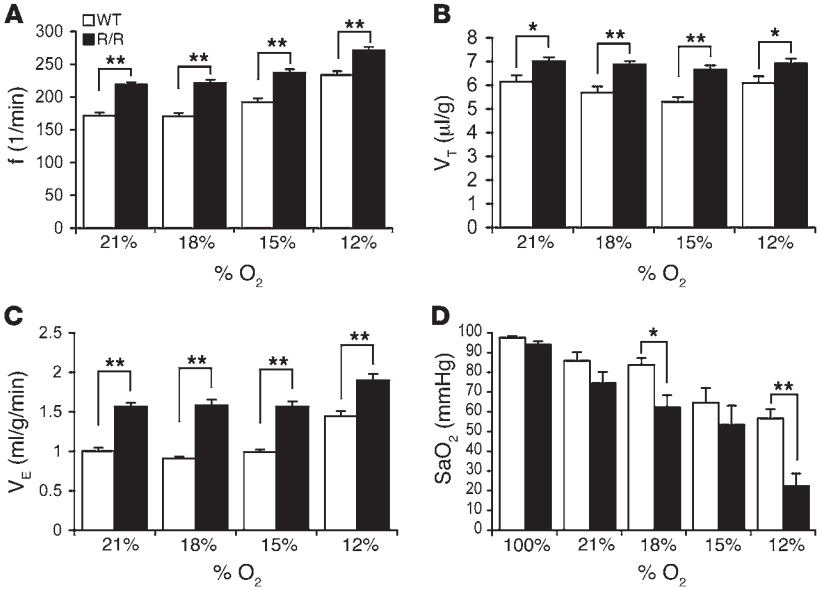

Figure 2
Baseline respiration is elevated in *Vhl*$^{R/R}$ mice. (**A**–**C**) Respiration was assessed in 7- to 8-month-old *Vhl*$^{R/R}$ mice and WT controls via whole body plethysmography under normoxia (21% O_2) and various levels of hypoxia (18%, 15%, or 12% O_2). The ventilatory rate (f, **A**) and tidal volume (V_T, **B**) increased approximately 1.2-fold in *Vhl*$^{R/R}$ mice under both normoxic and hypoxic conditions, corresponding to a 1.5-fold elevation in minute ventilation (V_E, **C**) (n = 42–48, *P < 0.05, **P < 0.001). In both WT and *Vhl*$^{R/R}$ mice, enhanced respiration was only observed under more severe hypoxia (12% O_2). (**D**) SaO_2 was decreased in *Vhl*$^{R/R}$ mice under hypoxic conditions, significantly at 18% (1.3-fold) and 12% O_2 (2.5-fold), indicative of impaired oxygen uptake (n = 4 mice per genotype with 3 measurements per O_2 level; *P < 0.02, **P < 0.005).

In agreement with this, both the average heart/body weight ratio (Figure 1C, 0.58% ± 0.02% versus 0.49% ± 0.02% in WT mice, n = 18–21, P < 0.009) and average RV wall thickness (Figure 1D, 430.5 ± 36.6 μm versus 283.4 ± 17.8 μm in WT mice, n = 11–17, P < 0.009) were significantly greater in these older *Vhl*$^{R/R}$ mice, confirming the presence of RV hypertrophy.

Increased pulmonary pressure is frequently marked by vascular remodeling due to enhanced muscularization of vessels within the lung, which contributes to vasoconstriction (29). The medial layer surrounding pulmonary vessels was not significantly altered in *Vhl*$^{R/R}$ lungs, as immunohistochemical staining for α-SMA and morphometric quantitation did not reveal significant differences in the medial thickness of *Vhl*$^{R/R}$ pulmonary vessels (Supplemental Figure 1, A–C; supplemental material available online with this article; doi:10.1172/JCI36362DS1). However, as shown in Figure 1E, the number of fully muscularized vessels (those completely surrounded by α-SMA staining) was significantly enhanced in *Vhl*$^{R/R}$ lungs at both 10 weeks (48.0% ± 2.2% versus 20.3% ± 4.3% in WT controls) and 7 months (59.8% ± 3.8% versus 38.3% ± 4.5% in WT mice). This was accompanied by a proportional decrease in nonmuscularized vessels in both age groups (21.3% ± 2.8% versus 52.8% ± 6.0% in WT lungs at 10 weeks; 12.5% ± 2.1% versus 19.6 ± 4.6% in WT lungs at 7 months; n = 4–5; P < 0.006) (Figure 1E). In agreement with this, total *Acta2* mRNA expression (which encodes for α-SMA) was increased in *Vhl*$^{R/R}$ lungs (Supplemental Figure 1D, 1.4-fold, P < 0.02).

Respiration is increased in Vhl$^{R/R}$ *mice*. In addition to pulmonary hypertension, both basal ventilation and hypoxic respiratory responses are elevated in Chuvash patients (27). We therefore examined respiration in 7- to 8-month-old *Vhl*$^{R/R}$ mice using whole body plethysmography to measure respiration frequency (f), tidal volume (V_T), and minute ventilation (V_E) under both normoxia and hypoxia (Figure 2, A–C). Baseline respiration was enhanced in *Vhl*$^{R/R}$ mice, similar to what is observed in Chuvash patients (27), with significant increases in all 3 parameters under normoxic conditions (21% O_2) compared with WT controls. These elevations in f (219.0 ± 3.4 versus 171.2 ± 5.4 in WT mice, n = 42–48, P < 0.001), V_T (7.0 ± 0.2 μl/g versus 6.2 ± 0.3 μl/g in WT mice, n = 43–48, P < 0.05), and V_E (1.6 ± 0.05 ml/g/min versus 1.0 ± 0.04 ml/g/min in WT mice, n = 43–48, P < 0.001) in *Vhl*$^{R/R}$ mice were maintained under hypoxic conditions. However, unlike in humans with this mutation (27), the respiratory response to hypoxia was not significantly enhanced in *Vhl*$^{R/R}$ animals. Mild to moderate hypoxia (18% and 15% O_2) did not induce respiratory changes above baseline (21% O_2) in either WT or *Vhl*$^{R/R}$ mice. In contrast, respiration was increased to a similar degree in both WT and *Vhl*$^{R/R}$ mice in response to more severe hypoxic stress (12% O_2) (Figure 2, A and C; for f, 271.0 ± 5.6 versus 233.6 ± 6.0 in WT mice; for V_E, 1.9 ± 0.08 ml/g/min versus 1.4 ± 0.07 ml/g/min in WT mice; n = 45, P < 0.001). This suggests that, although basal respiration is greater, respiratory sensitivity to hypoxia in mice is not dramatically altered by the R200W mutation.

To further examine respiratory efficiency and control, we analyzed arterial blood gas measurements from *Vhl*$^{R/R}$ mice and age-matched WT controls at 7 months of age (Table 1). There was no change in PaO_2 or O_2 saturation (SaO_2) levels in *Vhl*$^{R/R}$ mice at 21% O_2, indicating that mutant mice are not hypoxemic. However, SaO_2 levels were reduced in *Vhl*$^{R/R}$ mice under hypoxic conditions compared with WT controls, particularly at more severe hypoxia

Table 1
Normoxic arterial blood gas analysis

	WT	R/R	*P*
pH	7.2862 ± 0.02	7.2233 ± 0.01	P < 0.005
$PaCO_2$	37.9 ± 1.9	31.74 ± 1.3	P < 0.02
PaO_2	96.7 ± 4.6	103.2 ± 3.8	NS, P < 0.3
BE_{ecf}	−8.7 ± 0.5	−14.5 ± 0.6	P < 0.000003
HCO_3^-	17.93 ± 0.5	13.09 ± 0.5	P < 0.000003
TCO_2	19.1 ± 0.6	14.1 ± 0.6	P < 0.000003
SaO_2	96.1 ± 0.7	96.3 ± 0.6	NS, P < 0.8

Values represent mean ± SEM; n = 10 for WT and *Vhl*$^{R/R}$ (R/R) mice. P values represent comparisons of average R/R and average WT values. BE_{ecf}, base excess of the extracellular fluid — a measure of how acidic or basic the blood is.

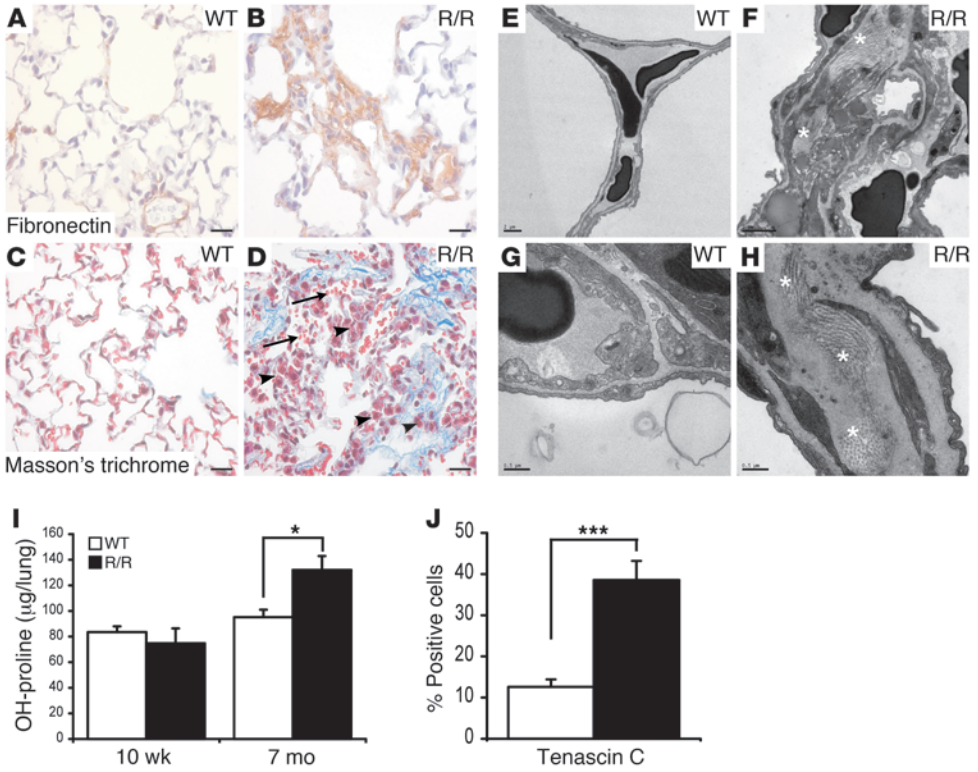

Figure 3

Fibrosis develops in older $Vhl^{R/R}$ lungs. (**A** and **B**) Fibronectin deposition (brown) was dysregulated and enhanced in $Vhl^{R/R}$ lungs at 7 months of age (**B**). (**C** and **D**) These $Vhl^{R/R}$ lungs also displayed accumulation of collagen fibers (shown in blue), as visualized with Masson's trichrome. Abundant collagen staining was often localized adjacent to areas of hemorrhage (**D**, arrows) and mononuclear infiltration (**D**, arrowheads). (**E**–**H**) EM analysis also revealed an increase in collagen in older $Vhl^{R/R}$ lungs (**F** and **H**, asterisks), compared with WT controls (**E** and **G**). (**I**) Although there was no change in hydroxyproline levels in younger $Vhl^{R/R}$ lungs (10 weeks, $n = 4$), collagen deposition was increased (1.4-fold) in older mutant lungs (7 months, $n = 5$, $^*P < 0.02$), indicating the presence of fibrosis. (**J**) The number of tenascin C–positive cells was significantly greater (2.6-fold) in $Vhl^{R/R}$ lungs, suggesting an increase in fibroblasts compared with WT mice ($n = 5$, $^{***}P < 0.0008$). Scale bars: 20 μm (**A**–**D**), 2 μm (**E** and **F**), 0.5 μm (**G** and **H**).

(Figure 2D; for 18%, 62.4 ± 6.0 mmHg versus 83.8 ± 3.4 mmHg in WT mice, $P < 0.02$; for 15%, 53.4 ± 9.7 mmHg versus 64.6 ± 7.5 mmHg in WT mice; for 12%, 22.3 ± 6.4 versus 56.7 ± 4.7 mmHg in WT mice, $P < 0.005$; $n = 4$), demonstrating that oxygen uptake in mutant lungs is impaired. Additionally, arterial $PaCO_2$ values were significantly decreased (approximately 6 mmHg lower; 37.9 ± 1.9 versus 31.74 ± 1.3 in WT mice) in $Vhl^{R/R}$ mice compared with WT animals and were accompanied by reductions in arterial HCO_3^- and total CO_2 (TCO_2) levels (Table 1). These results are identical to the changes in arterial blood gases in Chuvash patients (27) and support the notion that the R200W *Vhl* mutation results in enhanced respiratory drive at baseline.

The R200W mutation promotes ECM deposition and pulmonary fibrosis. In order to investigate the mechanisms underlying the development of pulmonary hypertension in $Vhl^{R/R}$ mice, we evaluated the pathology of mutant lungs at 7–8 months of age. Of note, $Vhl^{R/R}$ lungs displayed more dramatic changes in the adventitial layer and in ECM protein regulation. For example, fibronectin deposition was enhanced and more disorganized in $Vhl^{R/R}$ lungs (Figure 3B), compared with that in WT controls, in which fibronectin was primarily localized around pulmonary blood vessels (Figure 3A). Furthermore, Masson's trichrome staining revealed focal areas of collagen accumulation within the alveolar space of $Vhl^{R/R}$ lungs (Figure 3D, blue staining), unlike in WT controls, in which typically only basement membranes of the alveolar epithelium stained for collagen (Figure 3C). These results suggest that the R200W mutation disrupts ECM regulation within the lung, resulting in pulmonary fibrosis. Interestingly, the increase in collagen in mutant lungs was frequently localized adjacent to areas of hemorrhage (Figure 3D, arrows) and macrophage infiltration (Figure 3D, arrowheads). Electron microscopy (EM) analysis also indicated the presence of abundant collagen deposition (both longitudinal bundles and in cross section) in the interstitial space surrounding vessels in $Vhl^{R/R}$ lungs, as indicated by asterisks in Figure 3F and at higher magnification in Figure 3H. Quantitation of pulmonary hydroxyproline (OH-proline) content confirmed a significant increase in total lung collagen (132.0 ± 10.9 μg/lung versus 95.1 ± 5.8 μg/lung in WT mice, $n = 5$, $P < 0.02$) and the presence of mild fibrosis in older $Vhl^{R/R}$ lungs at 7 months of age (Figure 3I). However, this enhanced collagen accumulation was not present in younger $Vhl^{R/R}$ mice at 10 weeks of age (Figure 3I; 74.8 ± 11.6 μg/lung versus 83.5 ± 4.7 μg/lung in WT mice, $n = 4$, NS: $P < 0.5$), indicating that fibrosis develops after the onset of pulmonary hypertension. Consistent with the pathology observed in older $Vhl^{R/R}$ mice, the number of cells positive for tenascin-C, which has been associated with pulmonary fibrosis (46), was 2.6-fold greater in mutant lungs at 7 months (Figure 3J, 38.6% ± 4.6% versus 12.6% ± 1.8% in WT mice, $n = 5$, $P < 0.0008$).

$Vhl^{R/R}$ lungs display hemorrhage and edema. In addition to pulmonary fibrosis, $Vhl^{R/R}$ lungs exhibited regions of mild to moderate hemorrhage (compare Figure 4, A and B, arrows). The degree of hemorrhage was quantitated by staining cytospins of bronchoalveolar lavage (BAL) fluid for hemosiderin, which is a marker of iron deposition or red blood cell phagocytosis and is commonly found in macrophages localized to areas of hemorrhage (Figure 4, C and D, asterisks). Although the number of hemosiderin-positive cells was only slightly increased at 10 weeks (10.8 ±1.9 cells versus 6.8 ± 2.1 cells in WT mice, $n = 10$, $P < 0.16$), there was a 4.8-fold increase in $Vhl^{R/R}$ lungs at 7 months (11.6 ± 4.4 cells versus 2.4 ± 0.6 cells in WT mice, $n = 10$, $P < 0.05$) (Figure 4E). The presence of hemorrhage suggested alveolar injury or endothelial

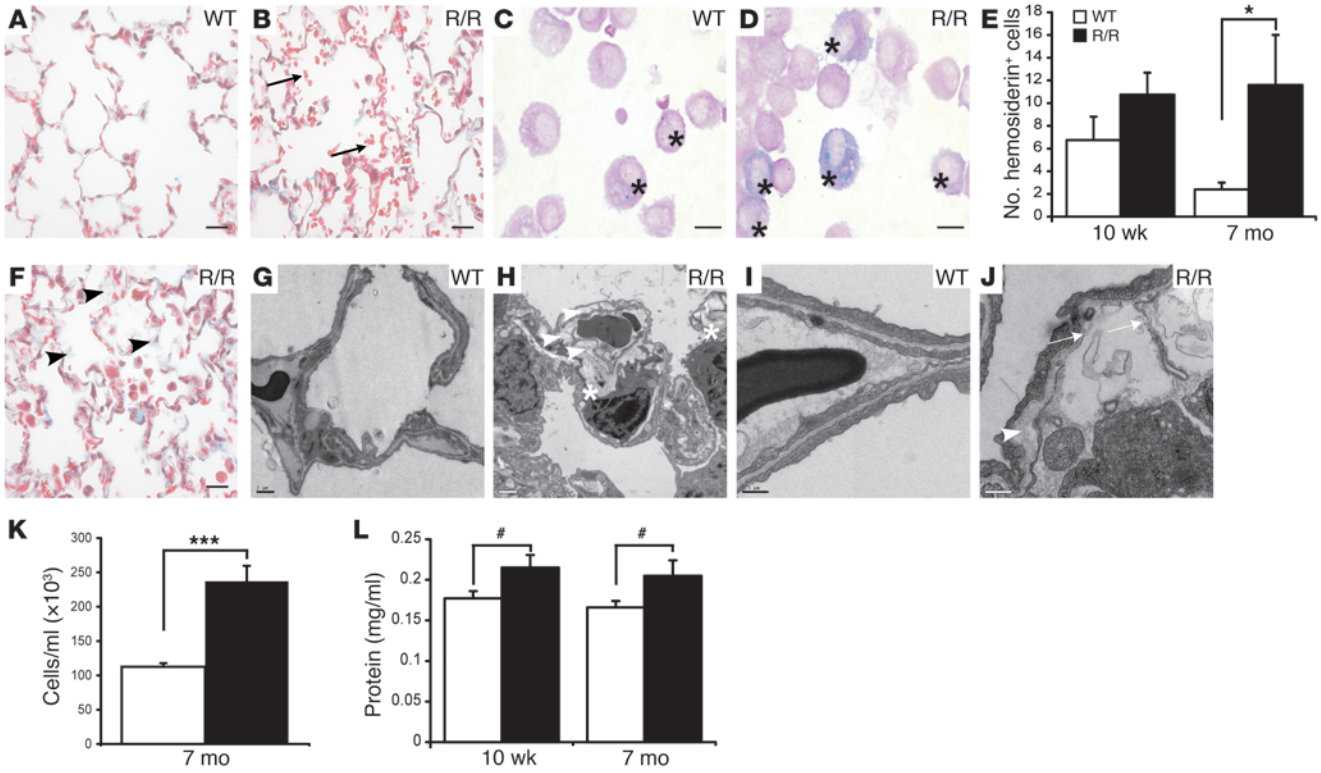

Figure 4

The R200W mutation causes pulmonary hemorrhage and edema. (**A** and **B**) Areas of mild to moderate hemorrhage were detected in *Vhl*$^{R/R}$ (**B**, arrows) compared with WT lungs (**A**) lungs at 7 months of age. (**C**–**E**) Hemorrhage was quantitated by scoring hemosiderin-positive cells in cytospins of BAL fluid (**C** and **D**, asterisks). The number of positive cells in *Vhl*$^{R/R}$ lungs was slightly increased (1.6-fold) at 10 weeks and significantly greater (4.8-fold) at 7 months of age (**E**, $n = 10$ per genotype, $^{*}P < 0.05$). (**F**) Mutant lungs also displayed edema, evidenced by thickening of alveolar walls (arrowheads). (**G**–**J**) EM revealed marked thickening of alveolar walls and expansion of the interstitial space, confirming the presence of edema in *Vhl*$^{R/R}$ lungs (**H** and **J**, arrowheads) compared with WT controls (**G** and **I**). Furthermore, *Vhl*$^{R/R}$ endothelium was sometimes irregular and discontinuous (**J**, arrows). Asterisks in **H** indicate collagen deposition. (**K** and **L**) The number of cells (**K**, 2.1-fold) was increased in *Vhl*$^{R/R}$ lungs, as was the total BAL protein concentration at both ages (**L**, 1.2-fold) ($n = 5$–10; $^{***}P < 0.0001$; $^{\#}P < 0.08$, trending toward significance). Sections in **A**, **B**, and **F** were stained with Masson's trichrome. Scale bars: 20 μm (**A**, **B**, and **F**), 10 μm (**C** and **D**), 2 μm (**G** and **H**), 0.5 μm (**I** and **J**).

dysfunction; however, staining for alveolar type II cells using the markers surfactant protein–B (SP-B) and surfactant protein–C (SP-C) was similar in WT and *Vhl*$^{R/R}$ lungs (Supplemental Figure 2, A–D), indicating that *Vhl*$^{R/R}$ alveolar epithelial architecture was maintained. Alveolar size (Supplemental Figure 2E) and capillary density (data not shown) were also not significantly different in *Vhl*$^{R/R}$ lungs compared with WT controls. In addition, we did not detect increased apoptosis in mutant lungs by cleaved caspase-3 staining (data not shown), indicating that epithelial cell survival was not significantly affected.

Histologic evaluation did suggest, however, a thickening of alveolar septa in *Vhl*$^{R/R}$ lungs, indicated by arrowheads in Figure 4F. This was supported by analysis of the pulmonary ultrastructure by EM, which revealed an expansion of *Vhl*$^{R/R}$ alveolar walls and the interstitial space (compare Figure 4, G and H), demonstrating the presence of edema in mutant animals (Figure 4, H and J, arrowheads). Moreover, the endothelium lining *Vhl*$^{R/R}$ pulmonary vessels was thin, irregular, or discontinuous in some areas (Figure 4J, arrows). This disruption in the pulmonary endothelium resulted in significantly increased numbers of cells (Figure 4K, $237.1 \times 10^3 \pm 22.4 \times 10^3$ cells/ml versus $112.5 \times 10^3 \pm 5.3 \times 10^3$ cells/ml in WT mice, $n = 10$, $P < 0.0001$) and elevated total protein concentration (Figure 4L; 0.21 ± 0.02 mg/ml versus 0.17 ± 0.008 mg/ml in WT mice, $n = 9$–10, $P < 0.08$, trending toward significance) in the BAL fluid of 7-month-old *Vhl*$^{R/R}$ mice. Edema was also present in younger *Vhl*$^{R/R}$ mice, as total BAL protein concentration at 10 weeks of age was greater compared with that in controls (Figure 4L; 0.22 ± 0.02 mg/ml versus 0.18 ± 0.009 mg/ml in WT mice, $n = 5$, $P < 0.08$, trending toward significance). EM analysis of 10-week-old *Vhl*$^{R/R}$ lungs also revealed the presence of expanded interstitial space and convoluted endothelial cells (data not shown). Therefore, pulmonary endothelial integrity is compromised in the presence of the R200W *Vhl* mutation, leading to hemorrhage and edema and likely also contributing to the pulmonary hypertension phenotype.

Increased macrophage infiltration in Vhl$^{R/R}$ *lungs.* As stated above, we observed enhanced inflammatory cell recruitment, primarily of macrophages, to *Vhl*$^{R/R}$ lungs (Figure 3D), often in regions of hemorrhage and edema. In comparison to WT lungs (Figure 5A), macrophages with abundant, pink-staining cytoplasm were easily identified in H&E sections of *Vhl*$^{R/R}$ lungs, usually occurring in clusters (Figure 5B, arrowheads). These cells were sometimes

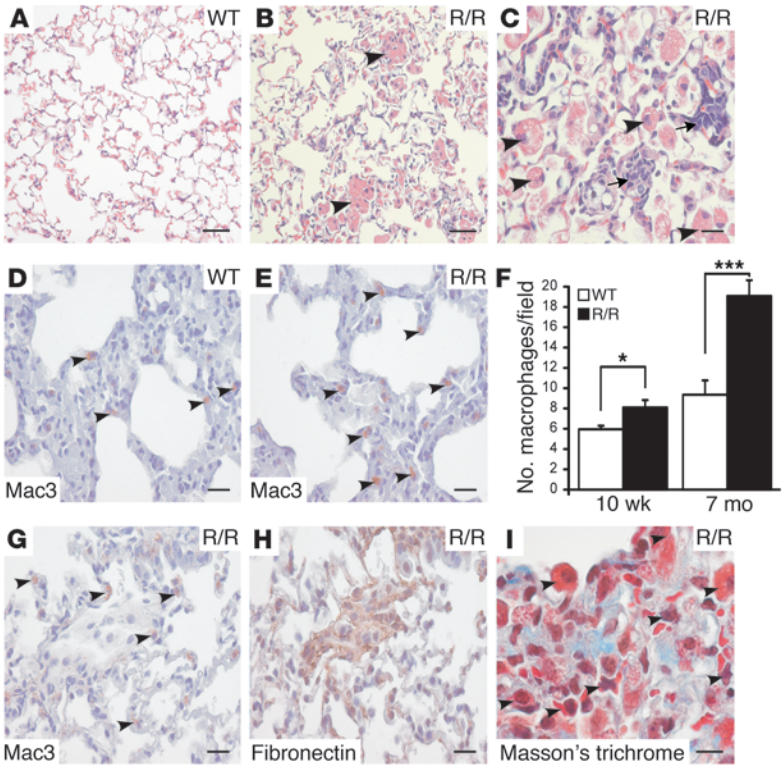

Figure 5
Macrophage infiltration is increased in $Vhl^{R/R}$ lungs. (**A**–**C**) Compared with WT lungs (**A**), $Vhl^{R/R}$ lungs displayed patches of infiltrating macrophages at 7 months of age (**B** and **C**, arrowheads). These cells were sometimes associated with lymphocytes (**C**, arrows) and contained vacuoles suggesting active phagocytosis (**C**). (**D**–**F**) Mac-3 staining (**D** and **E**, brown, arrowheads) demonstrated increased macrophages in $Vhl^{R/R}$ lungs at both 10 weeks and 7 months (**E**), as confirmed by quantitation (**F**, 1.4- and 2-fold increase, respectively, $n = 5$ per genotype, $^{*}P < 0.02$, $^{***}P < 0.001$). (**G**–**I**) Macrophage infiltration in $Vhl^{R/R}$ lungs (**G** and **I**, arrowheads) often colocalized with areas of enhanced fibronectin deposition (**H**, brown) and collagen accumulation (**I**, blue staining with Masson's trichrome). Scale bars: 50 μm (**A** and **B**), 20 μm (**C**–**E**, **G**, and **H**), 10 μm (**I**).

localized adjacent to lymphocytes (Figure 5C, arrows) and at higher magnification appeared to contain a frothy, vacuolar cytoplasm indicative of phagocytosis (Figure 5C, arrowheads). In agreement with this, a subset of $Vhl^{R/R}$ macrophages stained positively with Prussian blue, a marker of iron deposition (Supplemental Figure 3, A and B, blue staining). These results suggest that macrophages may be recruited to $Vhl^{R/R}$ lungs in response to endothelial injury (Figure 4J) to phagocytose red blood cells in hemorrhagic regions. In addition to macrophages, there was also a trend (although not statistically significant, $P < 0.2$) toward enhanced infiltration of mast cells into $Vhl^{R/R}$ lungs and increased numbers of neutrophils in $Vhl^{R/R}$ BAL fluid (Supplemental Figure 3, C and D).

The identity of these immune cells as macrophages was confirmed using 2 independent markers, CD68 (Supplemental Figure 3A) and Mac-3 (Figure 5, D and E, arrowheads). Macrophages were occasionally observed in WT lungs, but the number of Mac-3–positive cells was elevated 2-fold in $Vhl^{R/R}$ lungs at 7 months (Figure 5F; 19.1 ± 1.6 macrophages/field versus 9.4 ± 1.4 macrophages/field in WT mice, $n = 6$–9, $P < 0.001$). Increased macrophage infiltration was also detected in the lungs of younger $Vhl^{R/R}$ mice (Figure 5F; 8.1 ± 0.73 macrophages/field versus 5.9 ± 0.35 macrophages/field in WT mice, $n = 7$, $P < 0.02$), although the amount of infiltration was greater in older mutant animals. Furthermore, macrophages in $Vhl^{R/R}$ lungs often colocalized with increased fibronectin deposition (Figure 5G, arrowheads indicate macrophages, and Figure 5H, brown staining indicates fibronectin) and with collagen accumulation (Figure 5I, arrowheads point to macrophages, blue staining represents collagen). This finding suggests that the macrophages in $Vhl^{R/R}$ lungs may promote fibrosis through the stimulation of ECM production by fibroblasts.

HIF activity is upregulated in $Vhl^{R/R}$ lungs. HIF regulates the expression of many genes known to play a role in the pathogenesis of pulmonary hypertension (1). To investigate the molecular mechanisms underlying the pulmonary pathology in $Vhl^{R/R}$ mice, we evaluated the expression of a panel of HIF target genes in $Vhl^{R/R}$ lungs and age-matched WT controls (Figure 6, A and B). The expression of many HIF target genes was elevated in the lungs of older $Vhl^{R/R}$ mice at 7–8 months of age (Figure 6A, $n = 11$), as well as in younger mice at 10 weeks of age (Figure 6B, $n = 6$). For example, the expression of *Serpine1* (1.7-fold at both ages), *Edn1* (2.2-fold in older mice and 3.3-fold in younger mice), and *Pdgfb* ligand (1.4-fold at both ages) was significantly upregulated (Figure 6, A and B). ET-1 protein was also upregulated in the lungs of older $Vhl^{R/R}$ mice, as determined by ELISA analysis of total lung tissue (Figure 6C, 8.1 ± 1.6 pg/mg total protein versus 2.5 ± 0.4 pg/mg total protein in WT mice, $n = 5$, $P < 0.004$). In addition, the mRNA expression of stromal cell–derived factor–1α (*Cxcl12*), a chemokine that stimulates macrophage recruitment (47), was markedly increased at both ages (2.5-fold and 1.8-fold, respectively) in mutant lungs, as was that of hypoxia-induced mitogenic factor (*Retnla*, also known as *Himf*, 5.1-fold and 2.9-fold, respectively), a cytokine with proinflammatory and vasoconstrictive properties (Figure 6, A and B) (48, 49). This altered pattern of expression was limited to the lung, as we did not observe any significant changes in the expression of these genes in $Vhl^{R/R}$ hearts (data not shown).

Intriguingly, several of these genes, including *Serpine1* and *Edn1*, have been shown to be regulated by the HIF-2α isoform (5, 39). In contrast, the expression of the HIF-1α–specific target genes aldolase A (*Aldoa*) and *Pgk1* was not significantly changed in $Vhl^{R/R}$ compared with WT lungs (Figure 6, A and B), although there was a small change in *Pgk1* mRNA levels in $Vhl^{R/R}$ lungs at 10 weeks of age (Figure 6B). In agreement with this, the HIF-2α protein (and not HIF-1α) was selectively stabilized in $Vhl^{R/R}$ lungs compared with WT controls (Figure 6D). Importantly, the increase in normoxic

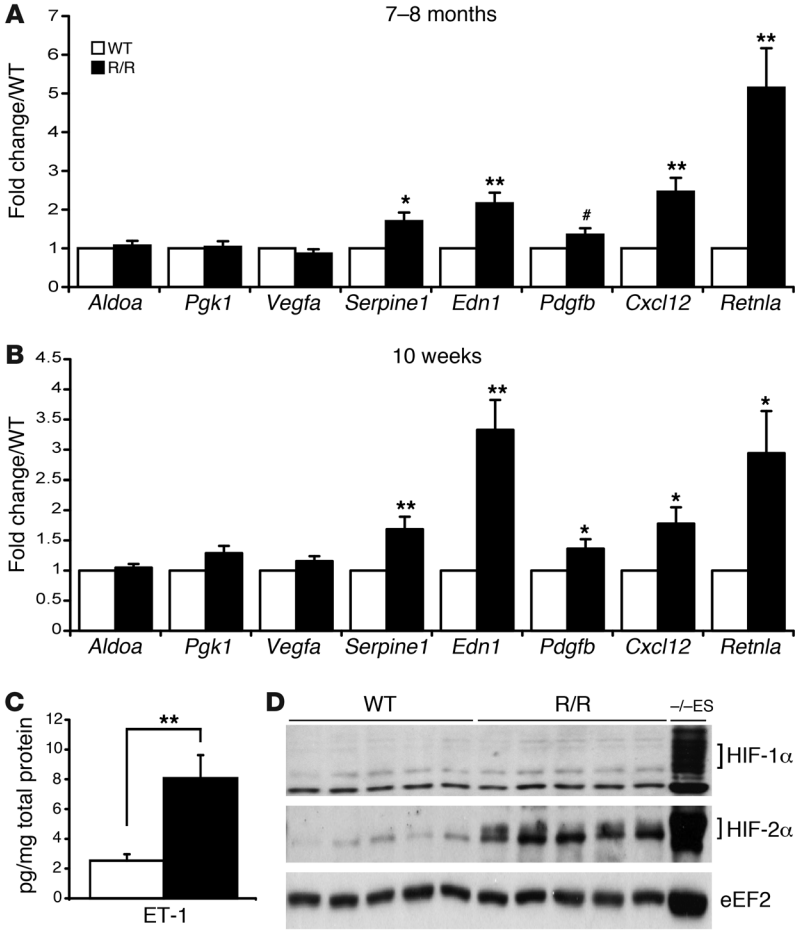

Figure 6
HIF target gene expression is increased in $Vhl^{R/R}$ lungs. (**A** and **B**) Pulmonary expression of HIF targets was determined by TaqMan real-time PCR. Many HIF target genes likely to contribute to the $Vhl^{R/R}$ pulmonary phenotype were upregulated, including *Serpine1*, *Edn1*, *Pdgfb*, and *Cxcl12*, in both older (7–8 months, **A**) and younger (10 weeks, **B**) mice. The expression of HIF-1α–specific targets *Aldoa* and *Pgk1* was unchanged in older $Vhl^{R/R}$ compared with WT lungs, whereas the mRNA levels of HIF-2α–preferential genes such as *Serpine1* were significantly elevated in $Vhl^{R/R}$ lungs (**A** and **B**) ($^{*}P < 0.03$, $^{**}P < 0.007$, $^{\#}P < 0.06$). (**C**) ET-1 protein expression was also increased in older $Vhl^{R/R}$ lungs, as determined by ELISA (3.2-fold, $^{**}P < 0.004$). (**D**) HIF-2α protein expression was increased in $Vhl^{R/R}$ lungs compared with WT controls; in contrast, HIF-1α was undetectable in both WT and $Vhl^{R/R}$ lungs.

HIF-2α levels was smaller than that seen in ES cells deficient for pVHL, emphasizing the more moderate effect of the R200W point mutation on pVHL function. Taken together, these data strongly support the notion that pulmonary hypertension in $Vhl^{R/R}$ mice results, at least in part, from enhanced pulmonary HIF-2α activity.

Polycythemia and pulmonary hypertension in $Vhl^{R/R}$ mice are dependent on increased HIF-2α activity. To further assess the relative contributions of each HIF-α isoform to the development of Chuvash disease, we tested whether decreased expression of either protein could rescue the polycythemic and pulmonary phenotypes. Given that $Hif1a^{-/-}$ and $Hif2a^{-/-}$ mice die in utero or at birth (50), mice heterozygous for either *Hif1a* or *Hif2a* were bred to $Vhl^{R/+}$ mice to generate $Vhl^{R/R}Hif1a^{+/-}$ and $Vhl^{R/R}Hif2a^{+/-}$ mice; mice at approximately 7 months of age were used for experiments. As shown in Figure 7A, $Vhl^{R/R}$ hematocrit levels were significantly greater than those of WT controls, as expected (56.1% ± 0.5% versus 49.6% ± 0.6% in WT mice, $n = 7$, $P < 0.0001$). Similarly, the hematocrit of $Vhl^{R/R}Hif1a^{+/-}$ mice was also elevated above WT levels (57.0% ± 1.4%, $n = 8$, $P < 0.0004$). However, loss of 1 *Hif2a* allele in $Vhl^{R/R}Hif2a^{+/-}$ mice resulted in a significant decrease in hematocrit compared with that of $Vhl^{R/R}$ mice (47.0% ± 0.9%, $n = 5$, $P < 0.0001$) and restored hematocrit to levels similar to those in WT (Figure 7A), supporting the hypothesis that HIF-2α activity is necessary for polycythemia. In accordance with this idea, serum EPO levels in $Vhl^{R/R}$ mice were also reduced to approximately WT levels in the presence of decreased *Hif2a*, but not *Hif1a* (Supplemental Figure 4).

Measurement of PA pressure in these mice revealed a similar dependency of the pulmonary hypertension phenotype on HIF-2α (Figure 7B). As discussed above (Figure 1A), PA pressure was significantly elevated in $Vhl^{R/R}$ mice compared with WT controls (31.8 ± 0.6 mmHg versus 18.3 ± 0.7 mmHg in WT mice, n = 20–23 measurements, $P < 0.0001$) but was unchanged by heterozygosity for *Hif1a* (30.0 ± 1.8 mmHg, $n = 19$, $P < 0.0001$ compared with WT mice). In contrast, although the PA pressure in $Vhl^{R/R}Hif2a^{+/-}$ mice was still significantly increased over WT levels (24.8 ± 0.6 mmHg, $n = 22$, $P < 0.0001$), there was a partial and statistically significant reduction in PA pressure compared with that in $Vhl^{R/R}$ mice (Figure 7B, $P < 0.0001$, indicated by asterisks). HIF-2α may also play an important role in the development of RV hypertrophy; RV wall thickness was diminished in $Vhl^{R/R}Hif2a^{+/-}$ mice, but not in $Vhl^{R/R}Hif1a^{+/-}$ mice, compared with $Vhl^{R/R}$ animals (Figure 7, C and D, 334.1± 23.1 μm in $Vhl^{R/R}Hif2a^{+/-}$ mice, 425.0 ± 43.0 μm in $Vhl^{R/R}$ mice, 436.1 ± 28.4 μm in $Vhl^{R/R}Hif1a^{+/-}$ mice, 322.4 ± 15.8 μm in WT mice, n = 4–6).

Similarly, HIF-2α, more so than HIF-1α, appears to be involved in pulmonary vascular remodeling, as shown in Figure 7E. Analysis of α-SMA–stained pulmonary vessels revealed a partial but significant decrease in the proportion of fully muscularized vessels in $Vhl^{R/R}Hif2a^{+/-}$ lungs compared with $Vhl^{R/R}$ lungs (48.4% ± 1.6% in $Vhl^{R/R}Hif2a^{+/-}$ mice, 59.8% ± 3.8% in $Vhl^{R/R}$ mice, 38.3% ± 4.5% in WT mice, n = 4–5, $P < 0.03$). Furthermore, *Hif2a* heterozygosity was sufficient to increase the number of nonmuscularized vessels to near WT levels (19.5% ± 1.6% in $Vhl^{R/R}Hif2a^{+/-}$ mice, 12.5% ±2.1% in $Vhl^{R/R}$

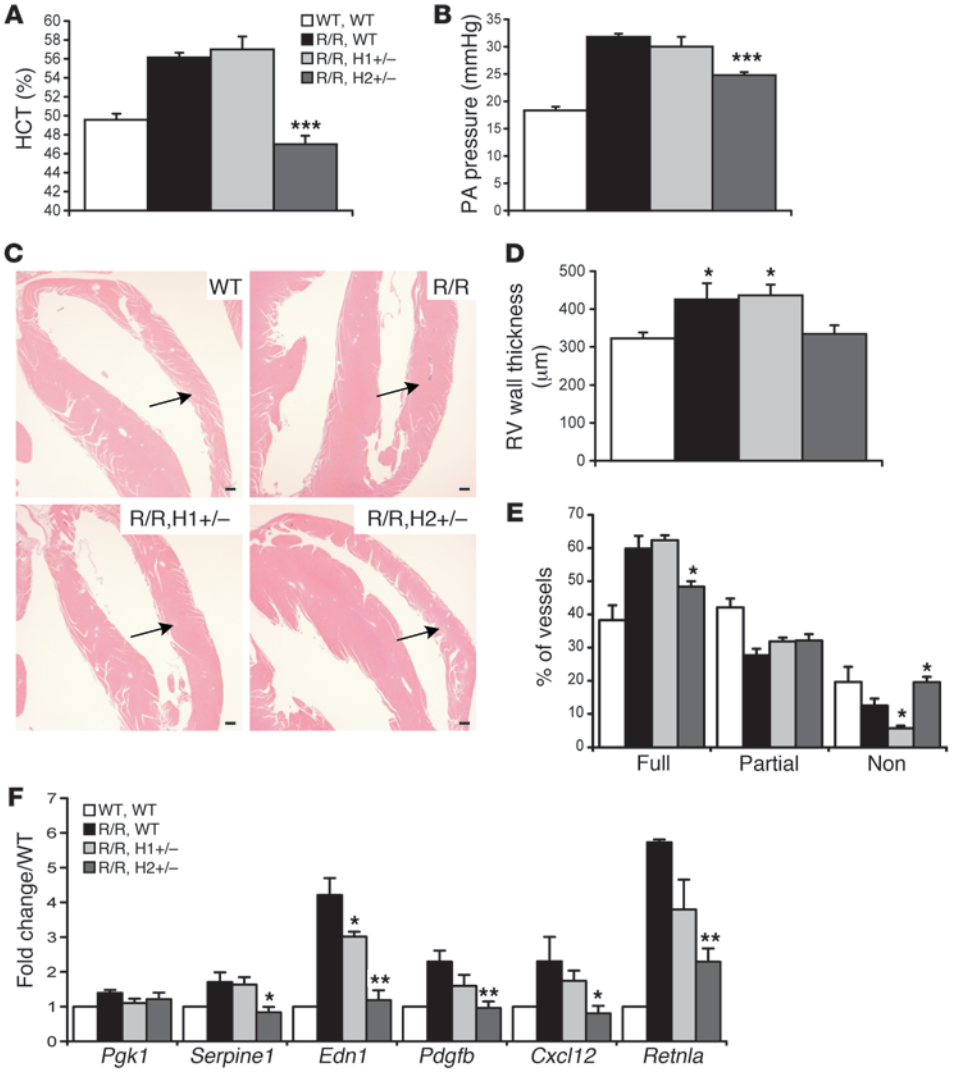

Figure 7
The polycythemic and pulmonary hypertension phenotypes are dependent on increased HIF-2α activity. (**A**) Loss of 1 allele of *Hif2a*, but not *Hif1a*, restored hematocrit levels in $Vhl^{R/R}$ mice to WT levels (n = 5–8, $^{***}P < 0.0001$ compared with $Vhl^{R/R}$ mice). H1+/–, $Hif1a^{+/-}$; H2+/–, $Hif2a^{+/-}$. (**B**) Systolic PA pressure was partially but significantly decreased in $Vhl^{R/R}Hif2a^{+/-}$ mice (n = 20–23, $^{***}P < 0.0001$ compared with $Vhl^{R/R}$ mice). (**C** and **D**) RV hypertrophy was also decreased in $Vhl^{R/R}Hif2a^{+/-}$ mice (**C**, arrows, and **D**, n = 4–6, $^{*}P < 0.05$ compared with WT hearts). (**E**) Only heterozygosity for *Hif2a* resulted in a significant decrease in fully muscularized pulmonary vessels (1.2-fold) and a concomitant increase in nonmuscularized vessels to WT levels (1.6-fold) (n = 4–5 per genotype, $^{*}P < 0.03$ compared with $Vhl^{R/R}$ lungs). (**F**) The expression of HIF target genes in $Vhl^{R/R}$ mice was reduced to nearly WT levels by heterozygosity for *Hif2a*, but not *Hif1a* (n = 5, $^{*}P < 0.03$, $^{**}P < 0.008$ compared with $Vhl^{R/R}$ lungs). Scale bars: 300 μm.

mice, 19.6% ± 4.6% in WT mice, $P < 0.03$ compared with $Vhl^{R/R}$ lungs). In contrast, the distribution of pulmonary vessels in $Vhl^{R/R}$ $Hif1a^{+/-}$ mice (for fully muscularized, 62.4% ± 1.5%; for nonmuscularized, 5.8% ± 0.8%) remained similar to that of $Vhl^{R/R}$ lungs.

In addition, analysis of pulmonary mRNA levels demonstrated that whereas *Hif1a* heterozygosity did not significantly alter the expression pattern in $Vhl^{R/R}$ lungs, loss of 1 allele of *Hif2a* resulted in significant downregulation of several key genes, including *Serpine1*, *Edn1*, *Pdgfb*, *Cxcl12*, and *Retnla* (Figure 7F; n = 5). We also confirmed that *Hif2a* mRNA levels were in fact decreased in $Vhl^{R/R}Hif2a^{+/-}$ lungs (Supplemental Figure 5). This result suggests that many of these genes may be preferentially induced by the HIF-2α isoform and further demonstrates that upregulation of HIF-2α is essential for the development of pulmonary hypertension in $Vhl^{R/R}$ mice.

Many, but not all, $Vhl^{R/R}$ pulmonary phenotypes are dependent on increased HIF-2α activity. Histologic analysis of lung pathology suggested that heterozygosity for either HIF isoform might also partially ameliorate other aspects of the $Vhl^{R/R}$ pulmonary phenotype (Figure 8A). Quantitation of hydroxyproline levels revealed that collagen deposition decreased 1.3- to 1.5-fold in $Vhl^{R/R}Hif1a^{+/-}$ and $Vhl^{R/R}Hif2a^{+/-}$ mice, suggesting that both HIF-α isoforms regulate fibrosis (Figure 8B, 65.21 ± 8.69 μg/lung in $Vhl^{R/R}Hif1a^{+/-}$ mice, 70.75 ± 13.25 μg/lung in $Vhl^{R/R}Hif2a^{+/-}$ mice, 94.61 ± 10.67 μg/lung in $Vhl^{R/R}$ mice, 57.9 ± 10.45 μg/lung in WT mice, n = 4–6). On the other hand, macrophage infiltration was not affected by heterozygosity for either *Hif1a* or *Hif2a* (Figure 8C, 11.9 ± 1.52 macrophages/field in $Vhl^{R/R}Hif1a^{+/-}$ mice, 12.4 ± 1.17 macrophages/field in $Vhl^{R/R}Hif2a^{+/-}$ mice, 13.2 ± 1.70 macrophages/field in $Vhl^{R/R}$ mice, 5.9 ± 0.63 macrophages/field in WT mice, n = 5, $P < 0.007$ compared with WT controls).

In contrast, however, the hemorrhage and edema phenotypes were partially resolved only in $Vhl^{R/R}Hif2a^{+/-}$ mice, implicating HIF-2α as the more relevant isoform in the loss of endothelial integrity observed in $Vhl^{R/R}$ mice. Whereas the degree of hemorrhage (as determined by hemosiderin staining) was unchanged with *Hif1a* heterozygosity compared with that in $Vhl^{R/R}$ lungs, the number of hemosiderin-positive cells was slightly reduced in $Vhl^{R/R}Hif2a^{+/-}$ mice (Figure 8D, 5.3 ± 2.1 cells in $Vhl^{R/R}Hif2a^{+/-}$ lungs, 9.9 ± 2.8 cells in $Vhl^{R/R}$ lungs, 11.2 ± 3.4 cells in $Vhl^{R/R}Hif1a^{+/-}$ lungs, 3.0 ± 0.7 cells in WT lungs, n = 5–7). Similarly, the edema phenotype was partially rescued in $Vhl^{R/R}Hif2a^{+/-}$, but not in $Vhl^{R/R}Hif1a^{+/-}$, mice. As shown in Figure 8E, the number of cells in BAL fluid was signifi-

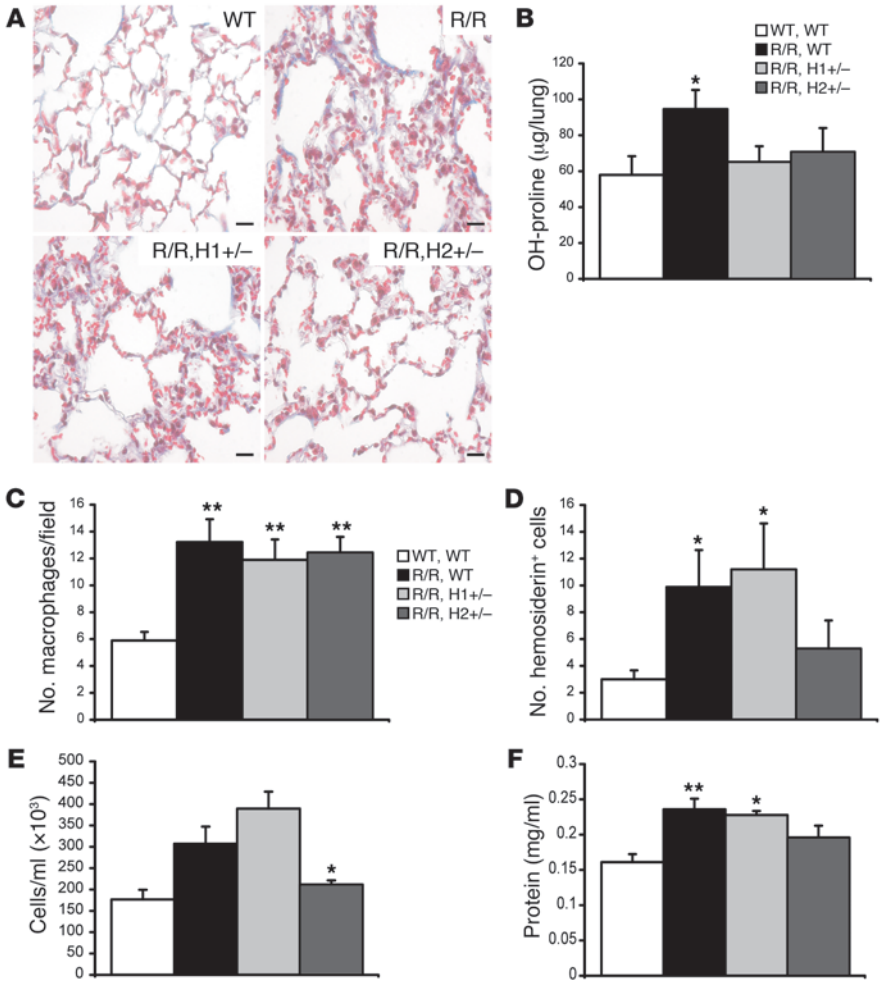

Figure 8
Some, but not all, *Vhl*$^{R/R}$ pulmonary phenotypes, are dependent on HIF-2α activity. (**A**) Representative lung images from each genotype suggest that neither *Hif1a* nor *Hif2a* heterozygosity completely restored WT pulmonary architecture (Masson's trichrome staining). (**B**) Hydroxyproline content was decreased in both *Vhl*$^{R/R}$ *Hif1a*$^{+/-}$ and *Vhl*$^{R/R}$ *Hif2a*$^{+/-}$ lungs compared with *Vhl*$^{R/R}$ (n = 4–6 per genotype, $^{*}P < 0.02$ compared with WT controls). (**C**) Macrophage infiltration was not significantly affected in either *Vhl*$^{R/R}$ *Hif1a*$^{+/-}$ or *Vhl*$^{R/R}$*Hif2a*$^{+/-}$ lungs (n = 5, $^{**}P < 0.007$ compared with WT). (**D**) In contrast, only *Hif2a* heterozygosity resulted in a partial rescue of the hemorrhage phenotype, as quantitated by hemosiderin staining (n = 5–7, $^{*}P < 0.01$ compared with WT controls). (**E** and **F**) Similarly, the number of cells in BAL from *Vhl*$^{R/R}$*Hif2a*$^{+/-}$ lungs was restored to near WT levels, suggesting a rescue of edema (**E**, n = 5, $^{*}P < 0.05$ compared with *Vhl*$^{R/R}$ lungs). There was also a trend toward decreased BAL protein concentration in *Vhl*$^{R/R}$*Hif2a*$^{+/-}$ lungs (**F**, n = 5, $^{*}P < 0.01$, $^{**}P < 0.003$ as compared with WT lungs). Scale bars: 20 μm.

cantly diminished to nearly WT levels only in *Vhl*$^{R/R}$*Hif2a*$^{+/-}$ mice ($211.4 \times 10^3 \pm 9.9 \times 10^3$ cells/ml in *Vhl*$^{R/R}$*Hif2a*$^{+/-}$ mice, $307.1 \times 10^3 \pm 40.2 \times 10^3$ cells/ml in *Vhl*$^{R/R}$ mice, $389.4 \times 10^3 \pm 39.7 \times 10^3$ cells/ml in *Vhl*$^{R/R}$*Hif1a*$^{+/-}$ mice, $176.7 \times 10^3 \pm 22.6 \times 10^3$ cells/ml in WT mice, n = 5, $P < 0.05$ compared with *Vhl*$^{R/R}$ mice). Furthermore, there was also a trend toward a reduction in total BAL protein concentration in *Vhl*$^{R/R}$*Hif2a*$^{+/-}$ mice (Figure 8F, 0.196 ± 0.017 mg/ml in *Vhl*$^{R/R}$*Hif2a*$^{+/-}$ mice, 0.236 ± 0.015 in *Vhl*$^{R/R}$ mice, 0.228 ± 0.006 in *Vhl*$^{R/R}$*Hif1a*$^{+/-}$ mice, 0.161 ± 0.011 in WT mice, n = 5). These results, combined with the partial rescue of pulmonary hypertension specifically by *Hif2a* heterozygosity (Figure 7B), suggest that hemorrhage and edema may be important factors in driving the increase in PA pressure in *Vhl*$^{R/R}$ mice.

Discussion

In addition to polycythemia, germline homozygosity for the R200W substitution is associated with development of pulmonary hypertension in patients with Chuvash disease (27, 28). To gain insight into how this mutation affects pulmonary physiology and to assess the contribution of HIF activity, we made use of our previously generated mouse model of Chuvash polycythemia (45). *Vhl*$^{R/R}$ mice also recapitulated the pulmonary hypertension phenotype, developing increased systolic PA pressure similar in magnitude to that seen in humans, as well as enhanced respiration under normoxia and induction of *Edn1* mRNA and ET-1 protein in the lung (27, 28). Altered cardiac and respiratory responses have also recently been described in *vhl*$^{-/-}$ zebrafish (51); however, this model is limited in its usefulness for studying the specific effects of the R200W mutation on mammalian pulmonary pathologies. Our results further validate *Vhl*$^{R/R}$ mice as a faithful model of Chuvash disease and support its usefulness for analysis of the pathogenesis of both polycythemia and pulmonary hypertension in humans.

Little is known about the mechanisms underlying the development of pulmonary hypertension associated with the R200W *VHL* mutation. Analysis of the *Vhl*$^{R/R}$ phenotype indicated the presence of increased pulmonary vessel muscularization, mild pulmonary fibrosis, edema, hemorrhage, and significant macrophage infiltration, highly similar to the effects induced by chronic exposure to hypoxia (29, 31). The majority of these pathologies were already present in younger *Vhl*$^{R/R}$ mice at 10 weeks of age, suggesting that they arise independently due to the effects of the R200W mutation on VHL function. In contrast, increased hydroxyproline content was only observed in older *Vhl*$^{R/R}$ animals; therefore, fibrosis does not contribute to the initiation of pulmonary hypertension. Rather, fibrosis likely develops in response to hemorrhage, edema, and impaired endothelial integrity and as a consequence of elevated HIF activity in older *Vhl*$^{R/R}$ lungs. Our data suggest that an HIF-mediated increase in pulmonary fibroblasts or myofibroblasts

induces fibrosis; however, additional work is necessary to fully elucidate this mechanism. There was a progressive increase in the degree of edema, hemorrhage, and inflammation in $Vhl^{R/R}$ animals with age, which ultimately led to a further elevation in pulmonary pressure and compensatory RV hypertrophy. The enhanced severity of pulmonary disease in older mice may result in part from feedback between different aspects of the phenotype. For example, the combination of increased PA pressure and loss of endothelial integrity produces edema and hemorrhage and could potentially enhance macrophage recruitment in response to endothelial injury (30, 52). Furthermore, infiltrating macrophages can mediate vascular remodeling and fibrosis via the stimulation of fibroblast proliferation, production of collagen, and expression of profibrotic factors (30, 53–55). Although lifespan was not significantly different in $Vhl^{R/R}$ mice, a small subset of mutant animals died unexpectedly, suggesting that the progressive nature of this disease could cause lethality. It will be important to determine whether fibrosis, hemorrhage, edema, and inflammation are also prominent pathological features in the lungs of human patients with Chuvash polycythemia and whether inhibition of any of these processes could be of therapeutic benefit.

Similar to humans with Chuvash disease (27), the R200W mutation also resulted in increased normoxic respiration and decreased $PaCO_2$ levels in $Vhl^{R/R}$ mice. Unlike in human patients, hypoxic respiratory sensitivity was not dramatically enhanced in mutant animals, possibly due to species-specific differences. However, SaO_2 values declined with increasing hypoxic exposure, indicating that oxygen diffusion is impaired in $Vhl^{R/R}$ lungs, possibly due to obstruction of airspace by fibrotic lesions. This analysis suggests that intact pVHL is necessary for proper respiratory function. This effect may be HIF dependent, as several HIF targets, such as tyrosine hydroxylase (56) and EPO (57), are involved in the regulation of respiration.

Our findings strongly suggest that the pulmonary pathology in $Vhl^{R/R}$ mice results in large part from enhanced HIF activity in the lung. Many of the genes described here have been shown to be important in pulmonary hypertension in animal models or in human samples (32–37); however, our study demonstrates that the upregulation of HIF targets plays a direct role in the $Vhl^{R/R}$ pulmonary phenotype. For example, activation of ET-1 and PAI-1 would increase vascular resistance and promote pulmonary fibrosis and chronic inflammation (33, 35). In addition, upregulation of the proinflammatory chemokines SDF-1α and HIMF have been shown to direct the recruitment of circulating monocytes to the lung (47, 49). HIMF also functions as a vasoconstrictive factor (48) and has been shown to colocalize with HIF-2α in the mouse lung (58). Although it remains formally possible that the R200W mutation disrupts HIF-independent functions of pVHL as well, such as the regulation of ECM assembly (13, 59–61) and maintenance of intercellular junctions (62), upregulation of HIF activity is likely to be the dominant factor in the development of $Vhl^{R/R}$ pulmonary pathology.

Interestingly, the expression of HIF-1α–specific targets was not changed in $Vhl^{R/R}$ lungs, whereas HIF-2α–regulated genes such as *Serpine1* were induced, correlating with the selective stabilization of HIF-2α protein, which is expressed to a high degree in the lung (63–65). This finding supports the notion (45) that the R200W mutation preferentially dysregulates HIF-2α and that HIF-2α activity is critical for the maintenance of lung physiology. This idea is further strengthened by the development of pulmonary hypertension in humans with an activating mutation in *HIF2A* (66). The current study may also have implications for our understanding of the relative contributions of the 2 HIF-α isoforms to the regulation of target genes. The induction of several genes in $Vhl^{R/R}$ lungs, including *Pdgfb*, *Edn1*, *Cxcl12*, and *Retnla*, was abrogated or partially diminished by *Hif2a* heterozygosity, suggesting that these may represent additional HIF-2α–preferential targets.

More importantly, the finding that heterozygosity for *Hif2a*, but not *Hif1a*, partially rescued both the polycythemia and pulmonary hypertension in $Vhl^{R/R}$ mice provides strong genetic evidence that HIF-2α is the more critical isoform in the pathogenesis of Chuvash disease. *Hif2a*, unlike *Hif1a*, heterozygosity also protected against most of the other observed $Vhl^{R/R}$ pulmonary phenotypes, resulting in a partial reversal of vascular remodeling and a reduction in hemorrhage, edema, and fibrosis. However, fibrosis was also decreased in $Vhl^{R/R}Hif1a^{+/-}$ lungs despite the absence of any change in pulmonary pressure, again suggesting that pulmonary hypertension in $Vhl^{R/R}$ mice is not dependent on fibrosis. This result also suggests that maximal and possibly cooperative activity of both HIF-1α and HIF-2α is necessary to induce fibrosis in $Vhl^{R/R}$ lungs. Therefore, there may be a subtle increase in HIF-1α expression in $Vhl^{R/R}$ lungs (barely detectable as shown in Figure 6D), which may contribute to enhanced ECM deposition through the induction of targets such as *Edn1*, which was decreased in $Vhl^{R/R}Hif1a^{+/-}$ mice (Figure 7F); connective tissue growth factor (*Ctgf*); lysyl oxidase (*Lox*) (67); and fibronectin (*Fn1*). Further supporting this, *Fn1* mRNA expression was slightly increased (1.3-fold) in $Vhl^{R/R}$ mice, but was reduced to WT levels in both $Vhl^{R/R}Hif1a^{+/-}$ and $Vhl^{R/R}Hif2a^{+/-}$ mice (data not shown). Of note, the expression of 2 other profibrotic factors, TGF-β1 and TGF-α, was not significantly different in WT and $Vhl^{R/R}$ mice (data not shown).

In contrast to the other phenotypes, macrophage infiltration was still enhanced in $Vhl^{R/R}Hif1a^{+/-}$ and $Vhl^{R/R}Hif2a^{+/-}$ mice. This persistence of inflammation and of some degree of vascular remodeling (Figure 7E) may help to explain the remaining increase in PA pressure in $Vhl^{R/R}Hif2a^{+/-}$ mice. The lack of decreased infiltration may indicate that the activity of either HIF-α isoform can promote macrophage recruitment or that the remaining HIF-α expression in heterozygous mice is sufficient to induce pulmonary inflammation. In support of the latter, *Retnla* mRNA levels in $Vhl^{R/R}Hif2a^{+/-}$ lungs were still higher than in WT controls (Figure 7F). In addition, there may also be elevated expression of other cytokines, as we observed a trend toward increased expression of macrophage inflammatory protein–1α (*Ccl3*) and monocyte chemoattractant protein–1 (*Ccl2*) in $Vhl^{R/R}$ lungs that was not rescued by heterozygosity for either *Hifa* isoform (data not shown). The presence of macrophage recruitment even in the absence of significant ECM accumulation might suggest an uncoupling of the fibrotic and inflammatory phenotypes. Alternatively, it is possible that the stimulation of fibrosis by macrophages is dependent on HIF activity within these cells, which would be reduced in $Vhl^{R/R}Hif1a^{+/-}$ and $Vhl^{R/R}Hif2a^{+/-}$ mice.

Another interesting question is the relationship between the polycythemic and pulmonary hypertension phenotypes in $Vhl^{R/R}$ mice and Chuvash patients. Our findings indicate that pulmonary hypertension develops concomitant with, if not prior to, the onset of polycythemia in mutant animals. We hypothesize that these 2 distinct phenotypes arise independently in younger mice as the result of the combined activation of a broad panel of HIF-2α targets. However, each of these diseases could contribute to the progression of the other with increasing age. For example, elevated hematocrits in polycythemic $Vhl^{R/R}$ mice and the subsequent

increase in blood viscosity could result in increased PA pressure (68). Furthermore, this viscosity could also promote edema (68) and hemorrhage, which may in turn stimulate the recruitment of macrophages to phagocytose erythrocytes within the alveolar space. Increased serum EPO levels in $Vhl^{R/R}$ mice may also help to enhance normoxic ventilation (57). On the other hand, elevated pulmonary resistance results in impaired pulmonary blood flow and decreased cardiac efficiency (31), which might promote compensatory red blood cell production to ensure adequate oxygen delivery to the body. Therefore, pulmonary hypertension may contribute to the progressive increase in $Vhl^{R/R}$ hematocrit levels in older mice (45).

Our findings demonstrate that this mouse model of Chuvash polycythemia also faithfully recapitulates the pulmonary hypertension that develops in human patients. Furthermore, the R200W mutation and subsequent increase in HIF activity mimic many of the systemic effects of chronic hypoxic exposure. Additional analysis of the R200W mouse model will help to improve our understanding of the unique effects of this point mutation on pVHL functions, as well as providing insights into the role of HIF in pulmonary physiology and the impact of chronic HIF activation in cardiopulmonary pathology. Moreover, our results suggest that specific inhibition of HIF-2α or the combined inhibition of several of the genes described here may be of therapeutic benefit for the treatment of human Chuvash disease.

Methods

Animals. $Vhl^{R/R}$ mice were generated as previously described (45). $Hif1a^{+/-}$ and $Hif2a^{+/-}$ mice were provided by Peter Carmeliet of the Center for Transgene Technology & Gene Therapy, Leuven, Belgium. All procedures involving mice were performed in accordance with the NIH guidelines for use and care of live animals and were approved by the University of Pennsylvania IACUC.

Measurement of PA pressure. Following anesthetization with avertin, the trachea was cannulated, and mice were ventilated using a MiniVent Type 845 (Harvard Apparatus). The chest cavity was opened to expose the heart, and a Micro-Tip Catheter Transducer SPR-1000 (Millar Instruments) was inserted into the RV and subsequently threaded into the PA. Systolic PA pressure was then measured, recorded on a PowerLab 4/30 instrument (ADInstruments), and analyzed using Chart 5 Pro software (ADInstruments). The transducer was calibrated prior to obtaining measurements for each mouse, and the quality of the pressure wave was monitored. Pressure measurements associated with heart rates outside the range of 300–500 bpm were excluded from analysis. For each mouse, 2–4 measurements were analyzed, each corresponding to the average of 10–20 individual data points.

Measurement of hypoxic ventilatory responses. Respiration was measured by whole body plethysmography using a 150-ml chamber connected to a pneumotachometer (MLT1L Respiratory Flow Head, ADInstruments). Data were recorded and converted using the PowerLab 8/SP (ADInstruments) and analyzed using Chart 5 software (ADInstruments). The Pegas-400 MF Gas Mixer (Columbus Instruments) was used to expose mice to varying levels of O_2 (18%, 15%, or 12%) for 10 minutes at a time, each interspaced with 10 minutes of 21% O_2. Respiratory frequency (f, 1/min), V_T (μl), and V_E (μl/s) were measured. V_T and V_E were then normalized to body weight.

Arterial blood gas analysis. Arterial blood gas analysis of carotid blood was performed using G3+ cartridges with an i-STAT analyzer (both Abbott Laboratories). For blood SaO_2 measurements, mice were anesthetized with ketamine (100 mg/kg)/xylazine (20 mg/kg), and an Animal-Clip Transducer and Oximeter Pod were used to record SaO_2 values on a PowerLab 4/30 instrument (all ADInstruments). Two-point calibration (100% and 21% O_2) was performed before each animal was exposed to varying levels of oxygen (100%, 21%, 18%, 15%, and 12% O_2) as described above. Each hypoxic challenge was interspersed with 2 minutes of 21% O_2. SaO_2 values represent the average of 3 challenges at each oxygen level for each animal.

BAL analysis. BAL fluid was isolated from lungs as described previously (69). Total cell number in BAL fluid was quantitated using a Coulter counter (Beckman Coulter), and total BAL fluid protein was measured by using a BCA protein assay kit (Pierce). Hemorrhage was quantified by preparing cytospins of BAL fluid and staining these slides with Prussian blue (Sigma-Aldrich) to identify macrophages with blue granules, indicating the presence of iron. The number of hemosiderin-positive cells was quantitated from 10 high-power fields per slide. BAL neutrophils were scored based on morphology.

Quantitation of OH-proline. Fibrosis was quantitated by determination of whole lung hydroxyproline content. Each mouse lung was weighed and cut into 1-mm-thick sections, dried, and hydrolyzed with 2 ml of 6N HCl at 120°C for 16 hours in sealed glass tubes. The amount of hydroxyproline was then measured as previously described and values corrected for the dilution factor (70). Commercial hydroxyproline (hydroxy-L-proline, Sigma-Aldrich) was used to establish a standard curve.

Hematological analyses and EPO ELISA. Determination of hematocrit and quantitation of serum EPO levels were performed as previously described (45).

Tissue preparation and histological analyses. Lungs were inflated to full capacity by intratracheal instillation of 4% paraformaldehyde. The heart and lungs were excised, immersed in 4% paraformaldehyde for fixation at 4°C for a minimum of 24 hours, and subsequently dehydrated in ethanol. Immunohistochemistry was performed as previously described (45) on paraffin-embedded sections of lungs using antibodies to fibronectin (Sigma-Aldrich, 1:400), Mac-3 (BD Biosciences — Pharmingen, 1:25), α-SMA (Sigma-Aldrich, 1:500), tenascin-C (Millipore, 1:20), CD68 (Abcam, 1:300), and mast cell tryptase (Abcam, 1:200). Staining for SP-B and SP-C was performed by the University of Pennsylvania Mouse Cardiovascular Physiology and Microsurgery Core. Masson's trichrome staining and Prussian blue staining (both Sigma-Aldrich) were performed according to the manufacturer's protocols. Transmission EM analysis was performed by the University of Pennsylvania Biomedical Imaging Core Laboratory following fixation of lung sections in 4% paraformaldehyde and 1% glutaraldehyde. The number of macrophages was quantitated from 10 independent high-power fields per slide. RV wall thickness was quantitated using NIH ImageJ software (http://rsbweb.nih.gov/ij/).

Morphometric analysis of pulmonary vessels. Vessel muscularity was determined using α-SMA–stained lung sections, with 15–20 fields and at least 100 vessels scored per animal. Each vessel was categorized as fully muscular (completely surrounded by α-SMA staining), partially muscular, or nonmuscular (no α-SMA staining), and values were expressed as the percentage of total vessels. Percent medial thickness was determined using NIH ImageJ software on these same slides using a previously described method (71). Alveolar size was assessed using a modified version of the mean linear intercept method (72), in which a grid with 36 intercepts was overlaid onto digital images of lung sections. Each intercept was scored for the presence of either airspace or alveolar septa from at least 3 slides per animal and expressed as the percentage of total intercepts.

mRNA and protein analyses. Total RNA isolation, cDNA synthesis, and TaqMan real-time PCR were performed as previously described (45). Whole lung protein extracts were isolated in a buffer containing Tris pH 8.0, $CaCl_2$, and NP-40 using a tissue homogenizer (IKA Labortechnik) followed by centrifugation. Western blot analysis was performed on supernatants using antibodies for murine HIF-1α (73), murine HIF-2α (R&D Systems), and eEF2 (Cell Signaling Technology) to control for loading as previously described (45). Total lung ET-1 protein content was determined on homogenized lung samples using an ELISA kit (R&D Systems) according to the manufacturer's specifications.

Statistics. Statistical analyses were performed for selected pairs using Bonferroni's test or unpaired Student's *t* tests. One-tailed *t* tests were used for comparison of 7-month-old $Vhl^{R/R}$ and WT PA pressure and pulmonary gene expression and for ET-1 and serum EPO ELISAs; 2-tailed *t* tests were used for all other analyses, including those involving *Hifa* heterozygous mice. *P* values of less than 0.05 were considered statistically significant. Mean results are shown; error bars represent SEM.

Acknowledgments

The authors thank Jennifer Lam and Brian Keith for technical assistance and critical review of the manuscript. This work was supported by the Abramson Family Cancer Research Institute; NIH grants HL066310 (to M.C. Simon), HL075215 and HL064632 (to E.E. Morrisey), and 5R01-CA1333470-02 (to M. Christofidou-Solomidou); and Muscular Dystrophy Association grant MDA-4164 (T.S. Khurana). M.M. Hickey was supported by a Howard Hughes Medical Institute Predoctoral Fellowship in Biological Sciences. M.C. Simon is an Investigator of the Howard Hughes Medical Institute.

Received for publication November 25, 2009, and accepted in revised form December 14, 2009.

Address correspondence to: M. Celeste Simon, Howard Hughes Medical Institute, Abramson Family Cancer Research Institute, University of Pennsylvania School of Medicine, BRB II/III, Room 456, 421 Curie Boulevard, Philadelphia, PA 19104. Phone: 215.746.5532; Fax: 215.746.5511; E-mail: celeste2@mail.med.upenn.edu.

1. Semenza GL. Hypoxia-inducible factor 1: oxygen homeostasis and disease pathophysiology. *Trends Mol Med*. 2001;7(8):345–350.
2. Hu CJ, Wang LY, Chodosh LA, Keith B, Simon MC. Differential roles of hypoxia-inducible factor 1alpha (HIF-1alpha) and HIF-2alpha in hypoxic gene regulation. *Mol Cell Biol*. 2003;23(24):9361–9374.
3. Rankin EB, et al. Hypoxia-inducible factor-2 (HIF-2) regulates hepatic erythropoietin in vivo. *J Clin Invest*. 2007;117(4):1068–1077.
4. Gruber M, Hu CJ, Johnson RS, Brown EJ, Keith B, Simon MC. Acute postnatal ablation of Hif-2alpha results in anemia. *Proc Natl Acad Sci U S A*. 2007; 104(7):2301–2306.
5. Kim WY, et al. Failure to prolyl hydroxylate hypoxia-inducible factor alpha phenocopies VHL inactivation in vivo. *EMBO J*. 2006;25(19):4650–4662.
6. Raval RR, et al. Contrasting properties of hypoxia-inducible factor 1 (HIF-1) and HIF-2 in von Hippel-Lindau-associated renal cell carcinoma. *Mol Cell Biol*. 2005;25(13):5675–5686.
7. Lonergan KM, et al. Regulation of hypoxia-inducible mRNAs by the von Hippel-Lindau tumor suppressor protein requires binding to complexes containing elongins B/C and Cul2. *Mol Cell Biol*. 1998; 18(2):732–741.
8. Iwai K, et al. Identification of the von Hippel-Lindau tumor-suppressor protein as part of an active E3 ubiquitin ligase complex. *Proc Natl Acad Sci U S A*. 1999;96(22):12436–12441.
9. Lisztwan J, Imbert G, Wirbelauer C, Gstaiger M, Krek W. The von Hippel-Lindau tumor suppressor protein is a component of an E3 ubiquitin-protein ligase activity. *Genes Dev*. 1999;13(14):1822–1833.
10. Maxwell PH, et al. The tumour suppressor protein VHL targets hypoxia-inducible factors for oxygen-dependent proteolysis. *Nature*. 1999; 399(6733):271–275.
11. Ohh M, et al. Ubiquitination of hypoxia-inducible factor requires direct binding to the beta-domain of the von Hippel-Lindau protein. *Nat Cell Biol*. 2000;2(7):423–427.
12. Kaelin WG Jr. Molecular basis of the VHL hereditary cancer syndrome. *Nat Rev Cancer*. 2002;2(9):673–682.
13. Ohh M, et al. The von Hippel-Lindau tumor suppressor protein is required for proper assembly of an extracellular fibronectin matrix. *Mol Cell*. 1998; 1(7):959–968.
14. Bishop T, et al. Genetic analysis of pathways regulated by the von Hippel-Lindau tumor suppressor in Caenorhabditis elegans. *PLoS Biol*. 2004;2(10):e289.
15. Lee S, et al. Neuronal apoptosis linked to EglN3 prolyl hydroxylase and familial pheochromocytoma genes: developmental culling and cancer. *Cancer Cell*. 2005;8(2):155–167.
16. Tang N, Mack F, Haase VH, Simon MC, Johnson RS. pVHL function is essential for endothelial extracellular matrix deposition. *Mol Cell Biol*. 2006;26(7):2519–2530.
17. Ang SO, et al. Endemic polycythemia in Russia: mutation in the VHL gene. *Blood Cells Mol Dis*. 2002; 28(1):57–62.
18. Ang SO, et al. Disruption of oxygen homeostasis underlies congenital Chuvash polycythemia. *Nat Genet*. 2002;32(4):614–621.
19. Gordeuk VR, et al. Congenital disorder of oxygen sensing: association of the homozygous Chuvash polycythemia VHL mutation with thrombosis and vascular abnormalities but not tumors. *Blood*. 2004; 103(10):3924–3932.
20. Percy MJ, et al. Chuvash-type congenital polycythemia in 4 families of Asian and Western European ancestry. *Blood*. 2003;102(3):1097–1099.
21. Sergeyeva A, Gordeuk VR, Tokarev YN, Sokol L, Prchal JF, Prchal JT. Congenital polycythemia in Chuvashia. *Blood*. 1997;89(6):2148–2154.
22. Perrotta S, et al. Von Hippel-Lindau-dependent polycythemia is endemic on the island of Ischia: identification of a novel cluster. *Blood*. 2006; 107(2):514–519.
23. Pastore Y, et al. Mutations of von Hippel-Lindau tumor-suppressor gene and congenital polycythemia. *Am J Hum Genet*. 2003;73(2):412–419.
24. Pastore YD, et al. Mutations in the VHL gene in sporadic apparently congenital polycythemia. *Blood*. 2003;101(4):1591–1595.
25. Gordeuk VR, Prchal JT. Vascular complications in Chuvash polycythemia. *Semin Thromb Hemost*. 2006; 32(3):289–294.
26. Lewis MD, Roberts BJ. Role of the C-terminal alpha-helical domain of the von Hippel-Lindau protein in its E3 ubiquitin ligase activity. *Oncogene*. 2004; 23(13):2315–2323.
27. Smith TG, et al. Mutation of von Hippel-Lindau tumour suppressor and human cardiopulmonary physiology. *PLoS Med*. 2006;3(7):e290.
28. Bushuev VI, et al. Endothelin-1, vascular endothelial growth factor and systolic pulmonary artery pressure in patients with Chuvash polycythemia. *Haematologica*. 2006;91(6):744–749.
29. Stenmark KR, Fagan KA, Frid MG. Hypoxia-induced pulmonary vascular remodeling: cellular and molecular mechanisms. *Circ Res*. 2006;99(7):675–691.
30. Stenmark KR, Davie NJ, Reeves JT, Frid MG. Hypoxia, leukocytes, and the pulmonary circulation. *J Appl Physiol*. 2005;98(2):715–721.
31. Humbert M, et al. Cellular and molecular pathobiology of pulmonary arterial hypertension. *J Am Coll Cardiol*. 2004;43(12 Suppl S):13S–24S.
32. Semenza GL. Targeting HIF-1 for cancer therapy. *Nat Rev Cancer*. 2003;3(10):721–732.
33. Eitzman DT, et al. Bleomycin-induced pulmonary fibrosis in transgenic mice that either lack or overexpress the murine plasminogen activator inhibitor-1 gene. *J Clin Invest*. 1996;97(1):232–237.
34. Giaid A, et al. Expression of endothelin-1 in the lungs of patients with pulmonary hypertension. *N Engl J Med*. 1993;328(24):1732–1739.
35. Hocher B, et al. Pulmonary fibrosis and chronic lung inflammation in ET-1 transgenic mice. *Am J Respir Cell Mol Biol*. 2000;23(1):19–26.
36. Jankov RP, et al. A role for platelet-derived growth factor beta-receptor in a newborn rat model of endothelin-mediated pulmonary vascular remodeling. *Am J Physiol Lung Cell Mol Physiol*. 2005; 288(6):L1162–L1170.
37. Schermuly RT, et al. Reversal of experimental pulmonary hypertension by PDGF inhibition. *J Clin Invest*. 2005;115(10):2811–2821.
38. Yu AY, et al. Impaired physiological responses to chronic hypoxia in mice partially deficient for hypoxia-inducible factor 1alpha. *J Clin Invest*. 1999; 103(5):691–696.
39. Brusselmans K, et al. Heterozygous deficiency of hypoxia-inducible factor-2alpha protects mice against pulmonary hypertension and right ventricular dysfunction during prolonged hypoxia. *J Clin Invest*. 2003;111(10):1519–1527.
40. Shimoda LA, Manalo DJ, Sham JS, Semenza GL, Sylvester JT. Partial HIF-1alpha deficiency impairs pulmonary arterial myocyte electrophysiological responses to hypoxia. *Am J Physiol Lung Cell Mol Physiol*. 2001;281(1):L202–L208.
41. Shimoda LA, Fallon M, Pisarcik S, Wang J, Semenza GL. HIF-1 regulates hypoxic induction of NHE1 expression and alkalinization of intracellular pH in pulmonary arterial myocytes. *Am J Physiol Lung Cell Mol Physiol*. 2006;291(5):L941–L949.
42. Wang J, Weigand L, Lu W, Sylvester JT, Semenza GL, Shimoda LA. Hypoxia inducible factor 1 mediates hypoxia-induced TRPC expression and elevated intracellular Ca2+ in pulmonary arterial smooth muscle cells. *Circ Res*. 2006;98(12):1528–1537.
43. Schultz K, Fanburg BL, Beasley D. Hypoxia and hypoxia-inducible factor-1alpha promote growth factor-induced proliferation of human vascular smooth muscle cells. *Am J Physiol Heart Circ Physiol*. 2006;290(6):H2528–H2534.
44. Eul B, et al. Impact of HIF-1alpha and HIF-2alpha on proliferation and migration of human pulmonary artery fibroblasts in hypoxia. *FASEB J*. 2006; 20(1):163–165.
45. Hickey MM, Lam JC, Bezman NA, Rathmell WK, Simon MC. von Hippel-Lindau mutation in mice recapitulates Chuvash polycythemia via hypoxia-inducible factor-2alpha signaling and splenic erythropoiesis. *J Clin Invest*. 2007;117(12):3879–3889.
46. Kaarteenaho-Wiik R, Lakari E, Soini Y, Pollanen R, Kinnula VL, Paakko P. Tenascin expression and distribution in pleural inflammatory and fibrotic diseases. *J Histochem Cytochem*. 2000;48(9):1257–1268.
47. Phillips RJ, et al. Circulating fibrocytes traffic to the lungs in response to CXCL12 and mediate fibrosis. *J Clin Invest*. 2004;114(3):438–446.
48. Teng X, Li D, Champion HC, Johns RA. FIZZ1/RELMalpha, a novel hypoxia-induced mitogenic factor in lung with vasoconstrictive and angiogenic

properties. *Circ Res*. 2003;92(10):1065–1067.
49. Yamaji-Kegan K, Su Q, Angelini DJ, Champion HC, Johns RA. Hypoxia-induced mitogenic factor has proangiogenic and proinflammatory effects in the lung via VEGF and VEGF receptor-2. *Am J Physiol Lung Cell Mol Physiol*. 2006;291(6):L1159–L1168.
50. Hickey MM, Simon MC. Regulation of angiogenesis by hypoxia and hypoxia-inducible factors. *Curr Top Dev Biol*. 2006;76:217–257.
51. van Rooijen E, et al. Zebrafish mutants in the von Hippel-Lindau tumor suppressor display a hypoxic response and recapitulate key aspects of Chuvash polycythemia. *Blood*. 2009;113(25):6449–6460.
52. Sartori C, Allemann Y, Scherrer U. Pathogenesis of pulmonary edema: learning from high-altitude pulmonary edema. *Respir Physiol Neurobiol*. 2007; 159(3):338–349.
53. Frid MG, et al. Hypoxia-induced pulmonary vascular remodeling requires recruitment of circulating mesenchymal precursors of a monocyte/macrophage lineage. *Am J Pathol*. 2006;168(2):659–669.
54. Pinsky DJ, et al. Coordinated induction of plasminogen activator inhibitor-1 (PAI-1) and inhibition of plasminogen activator gene expression by hypoxia promotes pulmonary vascular fibrin deposition. *J Clin Invest*. 1998;102(5):919–928.
55. Mutsaers SE, Foster ML, Chambers RC, Laurent GJ, McAnulty RJ. Increased endothelin-1 and its localization during the development of bleomycin-induced pulmonary fibrosis in rats. *Am J Respir Cell Mol Biol*. 1998;18(5):611–619.
56. Czyzyk-Krzeska MF, Bayliss DA, Lawson EE, Millhorn DE. Regulation of tyrosine hydroxylase gene expression in the rat carotid body by hypoxia. *J Neurochem*. 1992;58(4):1538–1546.
57. Soliz J, et al. Erythropoietin regulates hypoxic ventilation in mice by interacting with brainstem and carotid bodies. *J Physiol*. 2005;568(Pt 2):559–571.
58. Wagner KF, et al. Hypoxia-induced mitogenic factor has antiapoptotic action and is upregulated in the developing lung: coexpression with hypoxia-inducible factor-2alpha. *Am J Respir Cell Mol Biol*. 2004; 31(3):276–282.
59. Stickle NH, Chung J, Klco JM, Hill RP, Kaelin WG Jr, Ohh M. pVHL modification by NEDD8 is required for fibronectin matrix assembly and suppression of tumor development. *Mol Cell Biol*. 2004; 24(8):3251–3261.
60. Grosfeld A, et al. Interaction of hydroxylated collagen IV with the von Hippel-Lindau tumor suppressor. *J Biol Chem*. 2007;282(18):13264–13269.
61. Kurban G, et al. Collagen matrix assembly is driven by the interaction of von Hippel-Lindau tumor suppressor protein with hydroxylated collagen IV alpha 2. *Oncogene*. 2008;27(7):1004–1012.
62. Calzada MJ, et al. von Hippel-Lindau tumor suppressor protein regulates the assembly of intercellular junctions in renal cancer cells through hypoxia-inducible factor-independent mechanisms. *Cancer Res*. 2006;66(3):1553–1560.
63. Ema M, Taya S, Yokotani N, Sogawa K, Matsuda Y, Fujii-Kuriyama Y. A novel bHLH-PAS factor with close sequence similarity to hypoxia-inducible factor 1alpha regulates the VEGF expression and is potentially involved in lung and vascular development. *Proc Natl Acad Sci U S A*. 1997;94(9):4273–4278.
64. Tian H, McKnight SL, Russell DW. Endothelial PAS domain protein 1 (EPAS1), a transcription factor selectively expressed in endothelial cells. *Genes Dev*. 1997;11(1):72–82.
65. Wiesener MS, et al. Widespread hypoxia-inducible expression of HIF-2alpha in distinct cell populations of different organs. *FASEB J*. 2003;17(2):271–273.
66. Gale DP, Harten SK, Reid CD, Tuddenham EG, Maxwell PH. Autosomal dominant erythrocytosis and pulmonary arterial hypertension associated with an activating HIF2 alpha mutation. *Blood*. 2008; 112(3):919–921.
67. Higgins DF, Kimura K, Iwano M, Haase VH. Hypoxia-inducible factor signaling in the development of tissue fibrosis. *Cell Cycle*. 2008;7(9):1128–1132.
68. Hasegawa J, et al. Altered pulmonary vascular reactivity in mice with excessive erythrocytosis. *Am J Respir Crit Care Med*. 2004;169(7):829–835.
69. Perkowski S, et al. Dissociation between alveolar transmigration of neutrophils and lung injury in hyperoxia. *Am J Physiol Lung Cell Mol Physiol*. 2006; 291(5):L1050–L1058.
70. Woessner JF Jr. The determination of hydroxyproline in tissue and protein samples containing small proportions of this imino acid. *Arch Biochem Biophys*. 1961;93:440–447.
71. Nakagawa Y, Kishida K, Kihara S, Funahashi T, Shimomura I. Adiponectin ameliorates hypoxia-induced pulmonary arterial remodeling. *Biochem Biophys Res Commun*. 2009;382(1):183–188.
72. Thurlbeck WM. Measurement of pulmonary emphysema. *Am Rev Respir Dis*. 1967;95(5):752–764.
73. Mansfield KD, et al. Mitochondrial dysfunction resulting from loss of cytochrome c impairs cellular oxygen sensing and hypoxic HIF-alpha activation. *Cell Metab*. 2005;1(6):393–399.